Structural Engineering and Mechanics, *Vol. 55, No. 2 (2015) 399-411*
DOI: http://dx.doi.org/10.12989/sem.2015.55.2.399

Buckling analysis of filament wound composite cylindrical shell for considering the filament undulation and crossover

Zhangxin Guo*[1,2], Xiaoping Han[2], Meiqing Guo[1] and Zhijun Han[1]

[1]*College of Mechanics, Taiyuan University of Technology, Taiyuan 030024, China*
[2]*Department of Engineering Mechanics, Northwestern Polytechnical University, Xi'an 710072, China*

(Received March 14, 2015, Revised May 29, 2015, Accepted June 17, 2015)

Abstract. The buckling equations of filament wound composite cylindrical shell are established. The coefficients K_{ij} and L_{ij} of the buckling equations are determined by solving the equations. The geometric analysis and the effective stiffness calculation for the fiber crossover and undulation region are respectively accomplished. Using the effective stiffness of the undulation region, the specific formulas of the coefficients K'_{ij} and L'_{ij} of the buckling equations are determined. Numerical examples of the buckling critical loads have been performed for the different winding angles and stacking sequences cylindrical shell designs. It can be concluded that the fiber undulation results in the less effect on the buckling critical loads P_{cr}. P_{cr} increases with the thickness-radius ratio. The effect on P_{cr} due to the fiber undulation is more obvious with the thickness-radius ratio. P_{cr} decreases with the length-radius ratio. The effect on P_{cr} due to the fiber undulation can be neglected when the ratio is large.

Keywords: filament winding composite; cylindrical shell; buckling; fiber undulation; external pressure

1. Introduction

Due to their considerably higher strength-to-weight ratio, filament winding composite cylinder structural forms are widely used in the aeronautic and astronautics industry, energy resources and transportation, oceanographic engineering et al. So buckling and stability analysis for composite cylinders are of great practical importance, and have received considerable attention.

Design and analysis for this kind of structures use the main assumptions of classical laminate theory (Erasmo *et al*. 2013, Sofiyev *et al*. 2014, Najafov *et al*. 2013). The influence of winding pattern on the mechanical response of filament wound glass/epoxy cylinders exposed to external pressure is studied by testing cylindrical specimens having stacked layers with coincident patterns in a hyperbaric testing chamber (Moreno and Douchin 2008). Anastasiadis and Simitses (1993) published the results for very long shells under external pressure and three construction materials: boron/epoxy, graphite/epoxy and Kevlar/epoxy. They concluded that for radius-to-thickness ratio of 7.5 most stacking sequences for all materials considered lead to buckling failure before strength failure.

Messager (2001) investigated the influence of the winding-induced thickness imperfections on

*Corresponding author, Ph. D., E-mail: woxintanran215@163.com

http://www.techno-press.org/?journal=sem&subpage=8 ISSN: 1225-4568 (Print), 1598-6217 (Online)

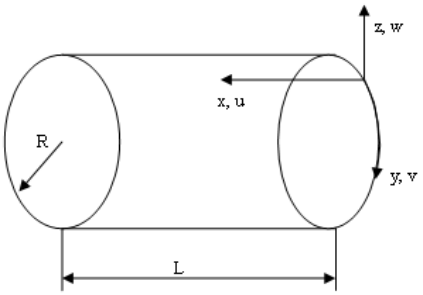

Fig. 1 Geometry of the cylindrical shell

to the elastic buckling load of laminated cylinders. A specific formulation of an analytical Sanders-type model for the buckling of imperfect laminated cylinders under external pressure was developed. Numerical tests were performed for different lamination cases of thin-walled, imperfect, carbon/epoxy cylinders. For the imperfect cylinders, the buckling pressure reductions obtained from the analytical model were in good agreement with FEM results. Several authors (Francesco *et al*. 2013, Azam 2004, Francesco *et al*. 2014, Sofiyev 2014) have carried out both analytical and experimental investigations on the buckling analysis of composite structures but most of the work is dedicated to very thin shells. In order to achieve the same strength as metals in some applications we need to use thicker cylinders. This in many instances pushes us to undertake the buckling and stability analysis on thick cylinders (Kardomateas and Philobox 1995, Chen *et al*. 2012).

Simitses (1996) presented a review on the problem of buckling of moderately thick, laminated, composite shells subjected to destabilizing loads. In all the works reported in the literature, the analysis is based on higher-order shear deformation shell theory and/or first-order shear deformation shell theory with or without a shear correction factor. The effect of stacking sequence, radius-to-thickness ratio and length-to-radius is assessed. Carvelli *et al*. (2001) presented some achievements related to the determination of the buckling strength of medium thick composite shells subjected to external pressure. An investigation based on experimental, analytical and numerical results is illustrated with reference to a specific model of an under-water vehicle. The collapse pressures were compared to the design values derived from the available recommendations and to the experimental result obtained in an off-shore test.

The filament-winding process introduces the fiber undulations and the nonorthogonality of the crossover geometry into thin-shell cylinders. The crossover of the fiber tows increase the likelihood of other manufacturing related defects such as resin-rich regions and fiber waviness. The fiber undulation regions possibile represent an initiation site for cracking. The increasing damage growth in the undulation region in turn lead to a stiffness decrease and the possibility of leaking in high interwoven structures.

In this paper, the buckling equations of filament wound composite cylinders are established. The coefficients K_{ij} and L_{ij} of the buckling equations are determined by solving the equations. The geometric analysis and the effective stiffness calculation for the fiber crossover and undulation region are respectively accomplished. Using the effective stiffness of the undulation region, the specific formulas of the coefficients K'_{ij} and L'_{ij} of the buckling equations are determined. Numerical examples of the buckling critical loads have been performed for the different winding angles and stacking sequences cylinders designs.

2. Buckling equations and calculation

The geometry and dimension of the cylindrical shell are shown in Fig. 1. In the above diagrammatic sketch, the *x*, *y* and *z* coordinates and the corresponding *u*, *v* and *w* displacements are measured in the axial, circumferential and radial directions, respectively, with respect to the cylindrical mean-surface.

The strain-displacement relations are as follows (Messager 2001, Shen 1995, Elghazouli *et al*. 1998)

$$\varepsilon_{xx} = \frac{\partial u}{\partial x} - z\frac{\partial^2 w}{\partial x^2} \tag{1a}$$

$$\varepsilon_{yy} = \frac{\partial v}{\partial y} + \frac{w}{R} + \frac{z}{R}\frac{\partial v}{\partial y} - z\frac{\partial^2 w}{\partial y^2} \tag{1b}$$

$$2\varepsilon_{xy} = \frac{\partial u}{\partial y} + \frac{\partial v}{\partial x} + \frac{2z}{R}\frac{\partial v}{\partial x} - 2z\frac{\partial^2 w}{\partial x \partial y} \tag{1c}$$

The displacement functions are given by Soldatos (1992)

$$\begin{cases} u = a_u \sin(\overline{m}x + \overline{n}y) \\ v = a_v \sin(\overline{m}x + \overline{n}y) \\ w = a_w \cos(\overline{m}x + \overline{n}y) \end{cases} \quad \text{with} \quad \begin{cases} \overline{m} = m\pi / L \\ \overline{n} = n / R \end{cases} \tag{2}$$

where $\{a_u \ a_v \ a_w\}^T$ is the eigen-displacement vector of the buckling problem; *m* and *n* are respectively the numbers of axial and circumferential half waves for characterizing the buckling mode, as shown in Fig. 2.

The orthotropic constitutive law for the kth composite ply is given by

$$\begin{Bmatrix} \sigma_{xx}^{(k)} \\ \sigma_{yy}^{(k)} \\ \sigma_{xy}^{(k)} \end{Bmatrix} = \begin{bmatrix} \overline{Q}_{11}^{(k)} & \overline{Q}_{12}^{(k)} & 0 \\ \overline{Q}_{12}^{(k)} & \overline{Q}_{22}^{(k)} & 0 \\ 0 & 0 & \overline{Q}_{66}^{(k)} \end{bmatrix} \begin{Bmatrix} \varepsilon_{xx}^{(k)} \\ \varepsilon_{yy}^{(k)} \\ 2\varepsilon_{xy}^{(k)} \end{Bmatrix} \tag{3}$$

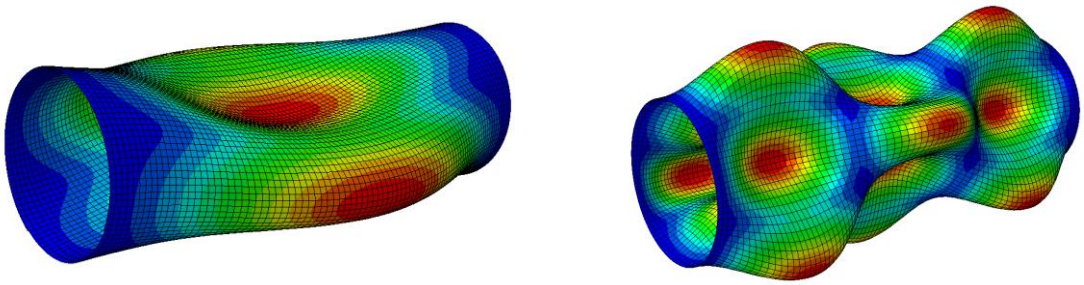

Fig. 2 The half waves mode of the buckling cylindrical shell

where $\overline{Q}_{ij}^{(k)}$ is the corresponding orthotropic, reduced, constitutive coefficients.

The force and moment resultants related to the mean-surface are expressed in the following form

$$\{N\}=\begin{Bmatrix}N_{xx}\\N_{yy}\\N_{xy}\end{Bmatrix}=\int_{-h/2}^{h/2}\begin{Bmatrix}\sigma_{xx}\\\sigma_{yy}\\\sigma_{xy}\end{Bmatrix}dz \tag{4a}$$

$$\{M\}=\begin{Bmatrix}M_{xx}\\M_{yy}\\M_{xy}\end{Bmatrix}=\int_{-h/2}^{h/2}\begin{Bmatrix}\sigma_{xx}\\\sigma_{yy}\\\sigma_{xy}\end{Bmatrix}zdz \tag{4b}$$

The three governing equations of equilibrium are as follows

$$\frac{\partial N_{xx}}{\partial x}+\frac{\partial N_{xy}}{\partial y}=0 \tag{5a}$$

$$\frac{\partial N_{yy}}{\partial y}+\frac{\partial N_{xy}}{\partial x}+\frac{1}{R}\frac{\partial M_{yy}}{\partial y}+\frac{1}{R}\frac{\partial M_{xy}}{\partial x}+\frac{p}{R}\left[v-R\frac{\partial w}{\partial y}\right]=0 \tag{5b}$$

$$\frac{\partial^2 M_{xx}}{\partial x^2}+2\frac{\partial^2 M_{xy}}{\partial x\partial y}+\frac{\partial^2 M_{yy}}{\partial y^2}-\frac{N_{yy}}{R}-p\left[\frac{R}{2}\frac{\partial^2 w}{\partial x^2}+R\frac{\partial^2 w}{\partial y^2}-\frac{\partial v}{\partial y}\right]=0 \tag{5c}$$

Substituting Eqs. (1) to (4) in Eq. (5), the characteristic equilibrium of buckling problem can be expressed as follows

$$\left[[K]+p[L]\right]\begin{Bmatrix}a_u\\a_v\\a_w\end{Bmatrix}=\begin{Bmatrix}0\\0\\0\end{Bmatrix} \tag{6}$$

where p is the external pressure, $[K]$ and $[L]$ are all the three-order matrix, the corresponding K_{ij} and L_{ij} (i, j=1, 2, 3) terms are given by the following formulas

$$K_{11}=A_{11}\overline{m}^2+A_{66}\overline{n}^2$$

$$K_{12}=\left(A_{12}+A_{66}+\frac{B_{12}+2B_{66}}{R}\right)\overline{m}\,\overline{n}$$

$$K_{13}=K_{31}=\frac{A_{12}}{R}\overline{m}+B_{11}\overline{m}^3+(B_{12}+2B_{66})\overline{m}\,\overline{n}^2$$

$$K_{21}=\left(A_{12}+A_{66}+\frac{B_{12}+B_{66}}{R}\right)\overline{m}\,\overline{n}$$

$$K_{22} = A_{22}\bar{n}^2 + A_{66}\bar{m}^2 + \frac{2B_{22}\bar{n}^2 + 3B_{66}\bar{m}^2}{R} + \frac{D_{22}\bar{n}^2 + 2D_{66}\bar{m}^2}{R^2}$$

$$K_{23} = \frac{A_{22}}{R}\bar{n} + (B_{12} + 2B_{66})\bar{m}^2\bar{n} + B_{22}\bar{n}^2 + \frac{(D_{12} + 2D_{66})\bar{m}^2\bar{n} + D_{22}\bar{n}^3}{R} + \frac{B_{22}\bar{n}}{R^2}$$

$$K_{32} = \frac{A_{22}}{R}\bar{n} + (B_{12} + 2B_{66})\bar{m}^2\bar{n} + B_{22}\bar{n}^2 + \frac{(D_{12} + 4D_{66})\bar{m}^2\bar{n} + D_{22}\bar{n}^3}{R} + \frac{B_{22}\bar{n}}{R^2}$$

$$K_{33} = \frac{A_{22}}{R^2} + \frac{2(B_{12}\bar{m}^2 + B_{22}\bar{n}^2)}{R} + D_{11}\bar{m}^4 + D_{22}\bar{n}^4 + 2(D_{12} + 2D_{66})\bar{m}^2\bar{n}^2$$

$$L_{11} = L_{12} = L_{13} = L_{21} = L_{31} = 0\,, \quad L_{22} = -1/R$$

$$L_{23} = L_{32} = -\bar{n}\,, \qquad L_{33} = -(\frac{\bar{m}^2}{2} + \bar{n}^2)R \tag{7}$$

where A_{ij}, B_{ij} and D_{ij} (i, j=1, 2, 6) terms are respectively the classical laminate stiffness coefficient of stretching, coupling and bending. The relevant calculating formulas are given by

$$A_{ij} = \sum_{k=1}^{n}(\overline{Q}_{ij})_k(z_k - z_{k-1})\,, B_{ij} = \frac{1}{2}\sum_{k=1}^{n}(\overline{Q}_{ij})_k(z_k^2 - z_{k-1}^2)\,, D_{ij} = \frac{1}{3}\sum_{k=1}^{n}(\overline{Q}_{ij})_k(z_k^3 - z_{k-1}^3) \tag{8}$$

The minimum generalized eigenvalue of Eq. (6) is calculated, and then the buckling critical load can be obtained.

3. Buckling equations of considering the filament undulation and crossover

3.1 Geometric analysis of fiber crossovers and undulations

Fiber tow crossovers and undulations within helical layers can be considered as a special form

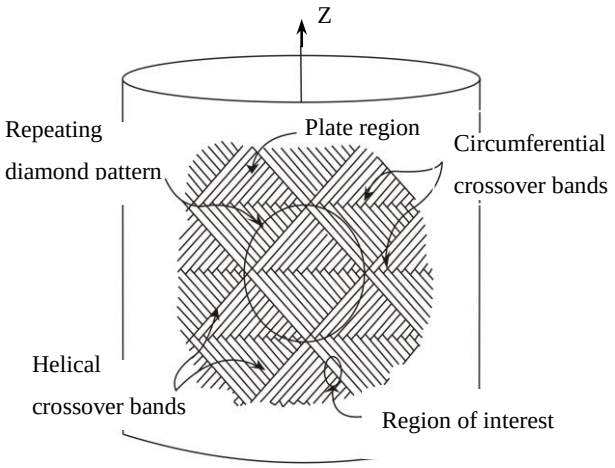

Fig. 3 The fiber winding patterns

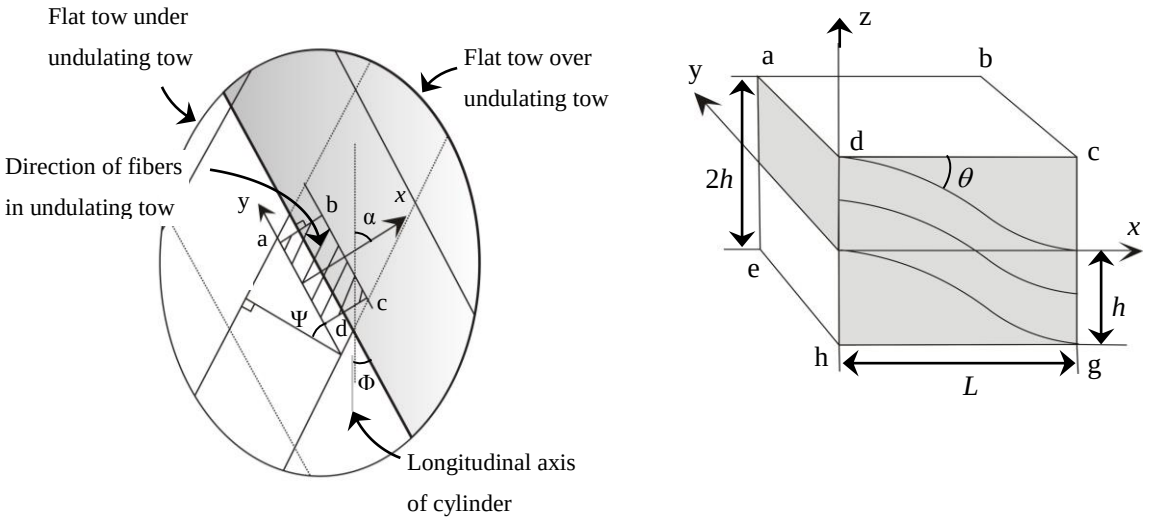

Fig. 4 The detailed structure of the fiber undulation

of defects (Guo *et al*. 2010, Jensen and Pai 1993). As shown in Fig. 3, the repetitive diamond-shaped patterns are formed on the filament-wound cylinders by two crossover layers. In a helically-wound layer, there are two regions containing fiber crossovers, namely the helical undulation region and the circumferential undulation region. The repetitive unit is divided into two areas: one is the uniformly laminated area where tows do not undulate, and the other is the undulation area that contains fiber crossovers and undulations. The helical and circumferential regions form the borders of the laminate region, which is in effect a laminate of unidirectional plies.

The detailed structure of fiber undulations is shown in Fig. 4. The *x*-*y*-*z* coordinate axis is along the principal direction of material, and the global cylinder coordinate is *r*-θ-*z*. The two important angles used for calculating the local stiffness are the filament-winding angle ϕ and the inclination angle θ due to the fiber undulation. It is noteworthy that ϕ is the in-plane transformation angle and θ is the out-of-plane transformation angle.

The mid-surface shape of the undulation fiber tow is determined by a cosine function as

$$h_u(x) = \frac{h}{2}\cos(\frac{\pi x}{L_u}) \tag{9}$$

where $h_u(x)$ is the centerline of the undulating fiber tow, h is the thickness of the fiber tow, x is the distance along the undulation, and L_u is the length of the undulation region.

The inclination angle θ of the undulating layer with respect to the filament-wound cylinder shell is then expressed by

$$\theta = \arctan(\frac{dh_u(x)}{dx}) \tag{10}$$

3.2 Calculation for the stiffness of the undulation region

The curved fiber-bundles can be regarded as an assembly of a large number of infinitesimal segments in the undulation region. Hence, the laminated plate theory is applicable for each segment along the undulation direction. Considering that θ is the angle between the principal coordinate of material and the off-axis coordinate (situated in the horizontal plane at a particular location, see Fig. 4), the principal stiffness C for the infinitesimal segment can be transformed into the off-axis stiffness C' by

$$[C'] = [T_\sigma]^{-1}[C][T_\varepsilon] \tag{11}$$

where T_σ is the transform matrix, i.e.

$$T_\sigma = \begin{bmatrix} l_1^2 & m_1^2 & n_1^2 & 2m_1n_1 & 2n_1l_1 & 2l_1m_1 \\ l_2^2 & m_2^2 & n_2^2 & 2m_2n_2 & 2n_2l_2 & 2l_2m_2 \\ l_3^2 & m_3^2 & n_3^2 & 2m_3n_3 & 2n_3l_3 & 2l_3m_3 \\ l_2l_3 & m_2m_3 & n_2n_3 & m_2n_3+m_3n_2 & n_2l_3+n_3l_2 & l_2m_3+l_3m_2 \\ l_3l_1 & m_3m_1 & n_3n_1 & m_3n_1+m_1n_3 & n_3l_1+n_1l_3 & l_3m_1+l_1m_3 \\ l_1l_2 & m_1m_2 & n_1n_2 & m_1n_2+m_2n_1 & n_1l_2+n_2l_1 & l_1m_2+l_2m_1 \end{bmatrix} \tag{12}$$

where l_1, m_1, n_1, l_2, m_2, n_2 are the directional cosines as afunction of θ angle respectively. The relationship between $[T_\sigma]$ and $[T_\varepsilon]$ is

$$[T_\varepsilon]^T = [T_\sigma]^{-1} \tag{13}$$

Thus, the material stiffness along the undulation varies with the point. Further, the 3D stiffness of the fiber tow at a point can be converted to the effective 2D form through the two angles of θ and φ. In addition, the assumptions of laminate theory are still applicable, i.e., γ_{xz}=0, γ_{yz}=0 and σ_z=0. Then, for an undulated layer, the 2D effective stiffness Q^*_{ij} is obtained as

$$Q^*_{ij} = C_{ij} - \frac{C_{i3}C_{3j}}{C_{33}} \qquad (i,j=1,2,6) \tag{14}$$

where C_{ij} are the 3D stiffness parameters of the undulating tow but in the local coordinate system.

Assume that the effective stiffness of the fiber undulation was already known, the equivalent stiffness of the whole filament composites is then calculated by using lamination theory

$$[A_{ij}(x), B_{ij}(x), D_{ij}(x)] = \sum_{m=1}^{n} \int_{h_{m-1}}^{h_m} \overline{Q}_{ij}(\varphi,\theta)[1, z, z^2]dz \qquad (i,j=1,2,6) \tag{15}$$

where A_{ij}, B_{ij} and D_{ij} are stiffness constants of stretching, stretching-bending coupling and bending, respectively. The average stiffness constants for the undulation of a filament-wound tow is then determined by numerically integrating as

$$[\overline{A}_{ij}(x), \overline{B}_{ij}(x), \overline{D}_{ij}(x)] = \frac{2}{L_u} \int_0^{L_u/2} [A_{ij}(x), B_{ij}(x), D_{ij}(x)]dx \tag{16}$$

In general, the stiffness constants of the combined layup are evaluated in terms of the mid-plane of the composite laminate. However, for filament-wound cylinders, the evaluation must be carried out in terms of a non-midplane by using the parallel axis theorem, and then transformed by

$$A'_{ij} = \sum_{k=1}^{M} A_{ij}^{(k)}$$

$$B'_{ij} = \sum_{k=1}^{M} (B_{ij}^{(k)} + d_k A_{ij}^{(k)})$$

$$D'_{ij} = \sum_{k=1}^{M} (D_{ij}^{(k)} + 2d_k B_{ij}^{(k)} + d_k^2 A_{ij}^{(k)})$$

$$d_k = \frac{T}{2} - (\sum_{m=1}^{k-1} t_m) - \frac{t_k}{2} \tag{17}$$

where the stiffness coefficients A'_{ij}, B'_{ij} and D'_{ij} are based on the reference surface (paralleling the filament-wound cylinder shell), and M is the number of filament-wound layers. d_k is the centerline distance of the k-th component from the reference surface. In Eq. (17), T is the thickness of the filament-wound cylinder while t_m and t_k are the thickness of the m-th and k-th component laminates, respectively.

After the stiffness constants of the undulating tows with respect to the local coordinate system are determined, they are then transformed to those in terms of the global coordinates of the cylinder by

$$\begin{aligned} [A] &= [T_\sigma]^{-1}[\overline{A}][T_\varepsilon] \\ [B] &= [T_\sigma]^{-1}[\overline{B}][T_\varepsilon] \\ [D] &= [T_\sigma]^{-1}[\overline{D}][T_\varepsilon] \end{aligned} \tag{18}$$

with the transformation angle α being

$$\alpha = 90^\circ - \phi \tag{19}$$

3.3 Buckling equations

After considering fiber undulation, the elastic orthotropic constitutive law for the kth composite ply is given by

$$\begin{Bmatrix} \sigma_{xx}^{(k)} \\ \sigma_{yy}^{(k)} \\ \sigma_{xy}^{(k)} \end{Bmatrix} = \begin{bmatrix} \overline{Q}_{11}^{(k)} & \overline{Q}_{12}^{(k)} & \overline{Q}_{16}^{(k)} \\ \overline{Q}_{12}^{(k)} & \overline{Q}_{22}^{(k)} & \overline{Q}_{26}^{(k)} \\ \overline{Q}_{16}^{(k)} & \overline{Q}_{26}^{(k)} & \overline{Q}_{66}^{(k)} \end{bmatrix} \begin{Bmatrix} \varepsilon_{xx}^{(k)} \\ \varepsilon_{yy}^{(k)} \\ 2\varepsilon_{xy}^{(k)} \end{Bmatrix} \tag{20}$$

According to Eqs. (1), (2), (4), (5), and (20), the final expression of the eigenvalue problem of

buckling for filament wound composite cylinders can be expressed as follows

$$\left[\left[K'\right]+p\left[L'\right]\right]\begin{Bmatrix}a_u\\a_v\\a_w\end{Bmatrix}=\begin{Bmatrix}0\\0\\0\end{Bmatrix} \tag{21}$$

The calculation of Eq. (21) leads to the lowest eigenvalue, then the critical external pressure P_{cr} can be obtained. The corresponding K'_{ij} and L'_{ij} (i, j=1,2,3) terms in Eq. (21) are detailed as follows

$$K'_{11}=A'_{11}\overline{m}^2+A'_{66}\overline{n}^2+2A'_{16}\overline{m}\overline{n}$$

$$K'_{12}=\left(A'_{12}+A'_{66}+\frac{B'_{12}+2B'_{66}}{R}\right)\overline{m}\overline{n}+A'_{16}\overline{m}^2+A'_{26}\overline{n}+\frac{2B'_{16}\overline{m}^2+B'_{26}\overline{n}^2}{R}$$

$$K'_{13}=K'_{31}=\frac{A'_{12}\overline{m}+A'_{26}\overline{n}}{R}+B'_{11}\overline{m}^3+(B'_{12}+2B'_{66})\overline{m}\overline{n}^2+3B'_{16}\overline{m}^2\overline{n}+B'_{26}\overline{n}^3$$

$$K'_{21}=\left(A'_{12}+A'_{66}+\frac{B'_{12}+B'_{66}}{R}\right)\overline{m}\overline{n}+A'_{26}\overline{n}^2+A'_{16}\overline{m}^2+\frac{B'_{16}\overline{m}^2+B'_{26}\overline{n}^2}{R}$$

$$K'_{22}=A'_{22}\overline{n}^2+A'_{66}\overline{m}^2+2A'_{26}\overline{m}\overline{n}+\frac{2B'_{22}\overline{n}^2+3B'_{66}\overline{m}^2+5B'_{26}\overline{m}\overline{n}}{R}+\frac{D'_{22}\overline{n}^2+2D'_{66}\overline{m}^2+(D'_{16}+2D'_{26})\overline{m}\overline{n}}{R^2}$$

$$K'_{23}=\frac{A'_{22}\overline{n}+A'_{26}\overline{m}}{R}+(B'_{12}+2B'_{66})\overline{m}^2\overline{n}+B'_{22}\overline{n}^3+B'_{16}\overline{m}^3+3B'_{26}\overline{m}\overline{n}^2+\frac{(D'_{12}+2D'_{66})\overline{m}^2\overline{n}+D'_{22}\overline{n}^3+D'_{16}\overline{m}^3+3D'_{26}\overline{m}\overline{n}^3}{R}+\frac{B'_{22}\overline{n}+B'_{26}\overline{m}}{R^2}$$

$$K'_{32}=\frac{A'_{22}\overline{n}+A'_{26}\overline{m}}{R}+(B'_{12}+2B'_{66})\overline{m}^2\overline{n}+B'_{22}\overline{n}^3+B'_{16}\overline{m}^3+3B'_{26}\overline{m}\overline{n}^2+\frac{(D'_{12}+4D'_{66})\overline{m}^2\overline{n}+D'_{22}\overline{n}^3+2D'_{16}\overline{m}^3+4D'_{26}\overline{m}\overline{n}^3}{R}+\frac{B'_{22}\overline{n}+2B'_{26}\overline{m}}{R^2}$$

$$K_{33}=\frac{A'_{22}}{R^2}+\frac{2(B'_{12}\overline{m}^2+B'_{22}\overline{n}^2)+4B'_{26}\overline{m}\overline{n}}{R}+D'_{11}\overline{m}^4+D'_{22}\overline{n}^4+2(D'_{12}+2D'_{66})\overline{m}^2\overline{n}^2+4(D'_{16}\overline{m}^3\overline{n}+D'_{26}\overline{m}\overline{n}^3)$$

$$L'_{11}=L'_{12}=L'_{13}=L'_{21}=L'_{31}=0,\quad L'_{22}=-1/R$$

$$L'_{23}=L'_{32}=-\overline{n},\quad L'_{33}=-\left(\frac{\overline{m}^2}{2}+\overline{n}^2\right)R \tag{22}$$

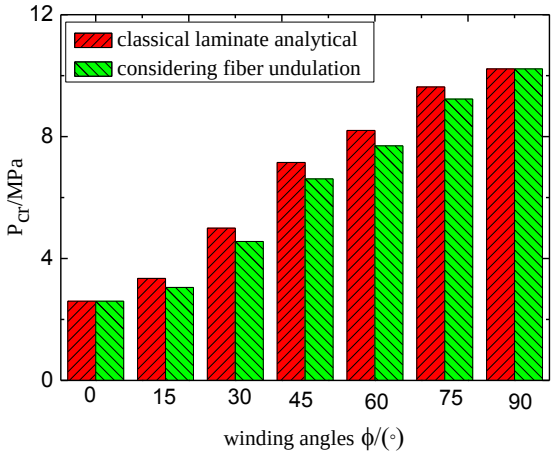

(a) stacking sequence $[\pm\phi]_{10}$

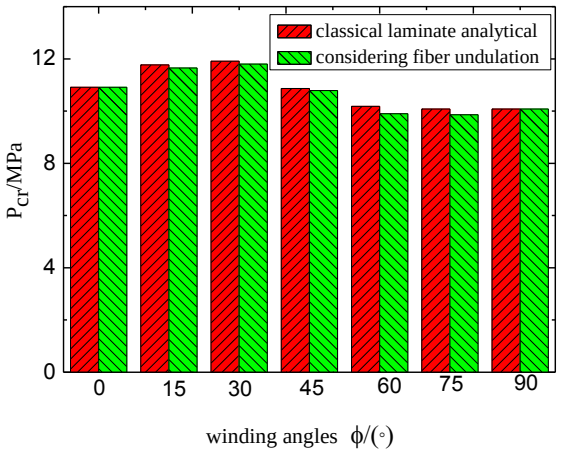

(b) stacking sequence $[90_5/\phi_{10}/90_5]$

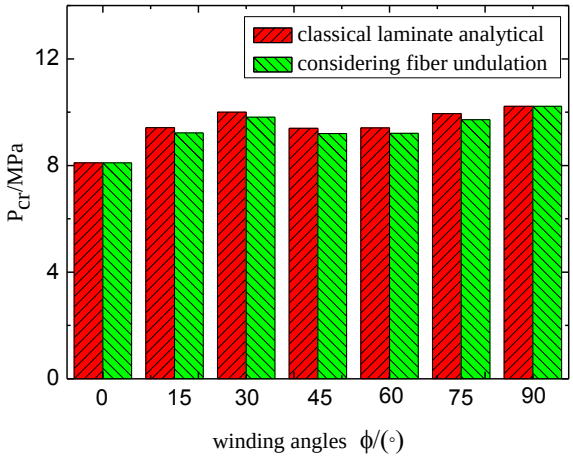

(c) stacking sequence $[90/\pm\phi/90/\pm\phi/90/\pm\phi/90]_s$

Fig. 5 Critical pressure for cylinders

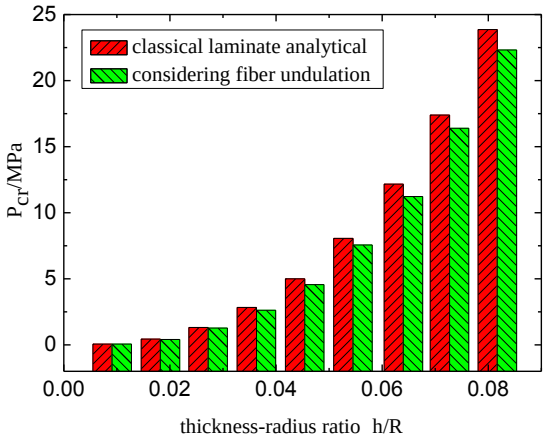

Fig. 6 Critical pressure for cylinders

where A'_{ij}, B'_{ij} and D'_{ij} (i, j=1,2,6) are the stiffness constants for the undulation region, and the specific calculation of these terms are detailed in Guo *et al*. (2010), Jensen and Pai (1993).

4. Calculating illustration and discussion

By using the above mentioned calculation model, the buckling critical loads of filament wound composite cylinders are obtained. The geometry dimensions of the considered cylinder are 76.2 mm in diameter, 228.6 mm in length and 3.46 mm in thickness. The thin-walled cylinder is composed of 10 composite cross-plies of equal thickness. The constituting material is a carbon fiber reinforced epoxy resin. The orthotropic in-plane mechanical characteristics are: E_1=156 GPa, E_2=9.65 GPa, G_{12}=5.47 GPa, ν_{12}=0.3, where subscripts 1 and 2 denote respectively the longitudinal and perpendicular directions of fibers.

Fig. 5 presents respectively the different winding angles and winding sequence cylinder designs, and the relevant buckling critical loads P_{cr}. It is seen that the fiber undulation results in the less effect on P_{cr}, and the effect due to the fiber undulation is much weakened with increasing the numbers of the hoop (90°) winding layers. From Fig. 5(a) for the $\pm\phi$ helical layer case, we can see that P_{cr} is strongly dependent on the winding angles, and become larger with winding angles. P_{cr} for ϕ=90° case is almost three times compared with ϕ=0° case, and increase rapidly between ϕ=30° to ϕ=70°. In contrast to Fig. 5 (b) and (c), we can see that, when the $\pm\phi$ layer is wound on the hoop (90°) layer and the winding sequence is different, the variation of P_{cr} is notable. For the winding sequence cylinder design $[90_5/\phi_{10}/90_5]$, P_{cr} increases at the beginning and attain the maximum at ϕ=30°, and then drops with the winding angle. For the cylinder design $[90/\pm\phi/90/\pm\phi/90/\pm\phi/90]s$, P_{cr} increases steeply at the beginning and then change gradually with the winding angle, and reach the maximum at ϕ=90°.

Fig. 6 depicts the effect of the thickness-radius ratio. P_{cr} increases with the thickness-radius ratio, and the changing level gradually increased. Besides, the effect on P_{cr} due to the fiber undulation is more obvious with the thickness-radius ratio. This may be explained as that the increase of thickness-radius ratio results in the relevant increase of helical layers, so the effect on

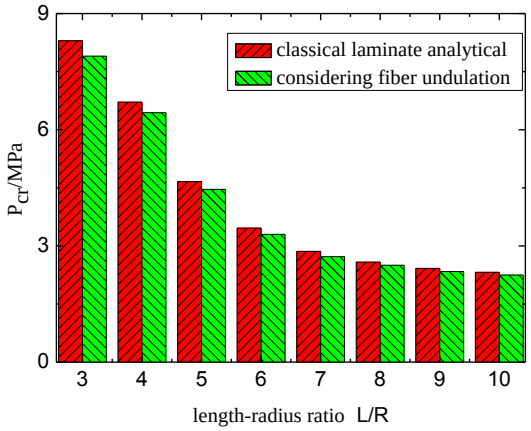

Fig. 7 Critical pressure for cylinders

P_{cr} due to the fiber undulation is enhanced.

Fig. 7 describes the effect of the length-radius ratio. P_{cr} decreases with the length-radius ratio, and the declination level is obvious. Moreover, the effect on P_{cr} due to the fiber undulation is more obvious when the length-radius ratio is small, and the effect can be neglected when the ratio is large.

5. Conclusions

• Considering the fiber undulations and nonorthogonality crossover, the buckling equations of filament wound composite cylindrical shell are established. Numerical examples of the buckling critical loads have been performed for the different winding angles and stacking sequences cylindrical shell designs.

• The fiber undulation results in the less effect on the buckling critical loads P_{cr}, and the effect is much weakened with increasing the numbers of the hoop (90°) winding layers.

• P_{cr} increases with the thickness-radius ratio. The effect on P_{cr} due to the fiber undulation is more obvious with the thickness-radius ratio.

• P_{cr} decreases with the length-radius ratio. The effect on P_{cr} due to the fiber undulation can be neglected when the ratio is large.

Acknowledgements

We gratefully acknowledge the financial support from the Qualified Personnel Foundation of Taiyuan University of Technology (QPFT) (No.tyutrc-201311a) and the Natural Science Foundation of China (Grant No. 51301117).

References

Anastasiadis, J.S. and Simitses, G.T. (1993), “Buckling of pressure-loaded, long, shear deformation,

cylindrical laminated shells", *Compos. Struct.*, **23**(3), 221-231.
Azam, T. (2004), "Delamination buckling and postbuckling in composite cylindrical shells under external", *Thin. Wall. Struct.*, **42**, 1379-1404.
Carvelli, V., Panzeri, N. and Poggi, C. (2001), "Buckling strength of GFRP under-water vehicles", *Part. B-Eng*., **32**, 89-101.
Chen, Z.P., Yang, L.C., Cao, G.W. and Guo, W.J. (2012), "Buckling of the axially compressed cylindrical shells with arbitrary axisymmetric thickness variation", *Thin. Wall. Struct.*, **60**, 38-45.
Elghazouli, A.Y., Chryssanthopoulos, M.K. and Spagnoli, A. (1998), "Experimental response of glass-reinforced plastic cylinders under axial compression", *Mar. Struct.*, **11**, 347-371.
Erasmo, V., Francesco, T. and Nicholas F. (2013), "General higher-order shear deformation theories for the free vibration analysis of completely doubly-curved laminated shells and panels", *Compos. Struct.*, **95**, 639-666.
Francesco, T., Nicholas, F., Erasmo, V. and Ferreira, A.J. (2013), "Radial basis function method applied to doubly-curved laminated composite shells and panels with a general higher-order equivalent single layer formulation", *Compos. Part. B-Eng*., **55**, 642-659.
Francesco, T., Nicholas, F., Erasmo, V. and Erasmo, C. (2014), "Static analysis of doubly-curved anisotropic shells and panels using CUF approach, differential geometry and differential quadrature method", *Compos. Struct.*, **107**, 675-697.
Guo, Z.X. and Han X.P. (2010), "Calculating stiffness of filament winding composite for considering the filament undulation and crossover", *Acta Materiae Compositae Sinica*, **27**(1), 179-184.
Jensen, D.W. and Pai, S.P. (1993), "Influence of local fiber undulations on the global buckling behavior of filament-wound cylinders", *J. Reinf. Plast. Comp.*, **12**, 865-875.
Kardomateas, G.A. and Philobox, M.S. (1995), "Buckling of thick orthotropic cylindrical shells under combined external pressure and axial compression", *AIAA J*, **33**, 1946-1953.
Messager, T. (2001), "Buckling of imperfect laminated cylinders under hydrostatic pressure", *Compos. Struct.*, **53**, 301-307.
Moreno, H.H. and Douchin, B. (2008), "Influence of winding pattern on the mechanical behavior of filament wound composite cylinders under external pressure", *Compos. Sci. Technol*., **68**, 1015-1024.
Najafov, A.M., Sofiyev, A.H. and Kuruoglu, N. (2013), "Torsional vibration and stability of functionally graded orthotropic cylindrical shells on elastic foundations", *Meccanica*., **48**, 829-840.
Shen, F.C. (1995), "A filament-wound structure technology overview", *Mater. Chem. Phys.*, **42**(2), 96-100.
Simitses, G.T. (1996), "Buckling of moderately thick laminated cylindrical shells: a review", *Compos. Part. B-Eng*., **27**, 581-587.
Sofiyev, A.H. and Kuruoglu, N. (2014), "Buckling and vibration of shear deformable functionally graded orthotropic cylindrical shells under external pressures", *Thin. Wall. Struct.*, **78**, 121-130.
Sofiyev, A.H. (2014), "The vibration and buckling of sandwich cylindrical shells covered by different coatings subjected to the hydrostatic pressure", *Compos. Struct.*, **117**, 124-134.
Soldatos, K.P. (1992), "Nonlinear analysis of transverse shear deformable laminated composite cylindrical shells", *J. Press. Vess-T. ASEM.*, **114**, 105-114.

CC